RSC Applied Interfaces

ROYAL SOCIETY OF CHEMISTRY

PAPER

View Article Online
View Journal

Cite this: DOI: 10.1039/d5lf00364d

Investigating interfacial chemistry for pre-passivated lithium-ion battery electrodes employing non-flammable methyl(2,2,2-trifluoroethyl)carbonate electrolytes

Lasse Dettmann, Florian Gebert and Andrew J. Naylor *

The transition to non-flammable electrolytes is essential to enhance the safety of rechargeable lithium-ion batteries in the context of rapid global electrification. However, these next-generation electrolytes often exhibit inferior electrochemical performance compared to conventional carbonate-based systems, hindering their practical application. Recent studies suggest that pre-passivating electrodes with conventional electrolytes can enhance performance for some next-generation electrolytes through interphase stabilization, yet a mechanistic understanding of this improvement remains to be established. In this work, we combine detailed electrochemical analysis with synchrotron-based hard X-ray photoelectron spectroscopy to investigate how pre-passivated electrodes influence the stability and performance of cells containing non-flammable electrolytes based on the solvent methyl(2,2,2-trifluoroethyl)carbonate (FEMC). We identify the anode solid electrolyte interphase (SEI) as the critical limiting factor towards use of FEMC electrolytes, with pre-passivation in conventional electrolytes significantly mitigating continuous electrolyte decomposition. Furthermore, our results show that the cathode electrolyte interphase (CEI) also plays a vital role, and that optimal performance is achieved by combining an SEI formed in a conventional electrolyte with a CEI formed in the FEMC electrolyte. These findings provide direct electrochemical and spectroscopic evidence for interphase-driven performance improvements, offering a practical pathway to advance non-flammable electrolyte technologies.

Received 19th November 2025,
Accepted 12th February 2026

DOI: 10.1039/d5lf00364d

rsc.li/RSCApplInter

1. Introduction

Carbonate ester-based liquid electrolytes are widely used in lithium-ion batteries (LIBs) in large part due to their ability to form a protective and ionically conductive solid electrolyte interphase (SEI) on the anode surface.[1–5] However, they pose significant safety risks when a cell is mechanically compromised or during a thermal event due to the electrolyte's high flammability.[6] Promising next-generation electrolyte concepts, including high-voltage-stable liquid electrolytes, non-flammable or low-flammability solvent systems, and solid-state or hybrid electrolytes, are being actively explored to improve the safety and performance of lithium-ion batteries. Among these, liquid electrolytes based on non-flammable fluorinated solvents such as methyl(2,2,2-trifluoroethyl)carbonate (FEMC) offer enhanced intrinsic safety while maintaining compatibility with conventional cell architectures. Flammability tests comparing a conventional carbonate-based electrolyte, FEMC, and FEMC containing 5 vol% carbonates are shown in Fig. S1, demonstrating the strongly reduced flammability of FEMC-based electrolytes even in the presence of minor carbonate residues. Nevertheless, such fluorinated electrolytes often fail to form a stable and passivating SEI on the anode.[7–9] The SEI formed by FEMC reduction typically results in a thick interphase with poor protective properties, which, together with solvent co-intercalation, contributes to increased cell resistance, poor reversibility, and continuous electrolyte decomposition.[7] This detrimental SEI formation accelerates capacity fading and reduces coulombic efficiency, compromising battery performance.

A common strategy to mitigate this issue is electrolyte engineering, where SEI-forming additives decompose before the main electrolyte, stabilizing the interphase.[1,2,4,10,11] However, this approach introduces complexity, as multiple additives may be required, and such additives can also be expensive. Some of these, such as linear carbonates including dimethyl carbonate (DMC), ethyl methyl carbonate (EMC), or diethyl carbonate (DEC), reintroduce highly flammable components into the electrolyte, especially at higher

Department of Chemistry-Ångström Laboratory, Uppsala University, SE-751 21, Uppsala, Sweden. E-mail: andy.naylor@kemi.uu.se

concentrations (>5%) or when used as co-solvents, *i.e.* >10%.[9,11] At lower concentrations, they often fail to sufficiently improve the performance of next-generation electrolytes.[7]

An alternative approach to maintain electrolyte safety and simplicity is pre-passivating the electrodes using a state-of-the-art electrolyte, such as LP57 (1 M $LiPF_6$ in a 3 : 7 v/v mixture of ethylene carbonate (EC) and ethyl methyl carbonate (EMC)), before transitioning to the non-flammable electrolyte for long-term operation. This strategy has been reported in the literature for various electrode materials and next-generation electrolytes, demonstrating performance improvements for some of the studied systems.[8,12–14] FEMC is a particularly interesting candidate in this context, as it exhibits poor cycling performance on its own, but significant improvements can be achieved after pre-passivating the electrodes, as our group has previously demonstrated.[8] In addition, the C-rate during pre-passivation has been found to strongly influence the SEI uniformity and thickness. Higher C-rates typically result in a non-uniform SEI, which fails to fully protect the electrode surface, whereas lower C-rates promote a more homogeneous and protective SEI layer.[12]

Despite these findings, the underlying mechanisms behind the improved long-term performance of pre-passivated electrodes with non-flammable electrolytes remain poorly understood. It is still unclear whether capacity fading primarily originates from the anode SEI or the cathode electrolyte interphase (CEI). Additionally, direct experimental evidence explaining why pre-passivated electrodes enhance galvanostatic cycling stability for FEMC based electrolytes is lacking.

To address these questions, we combine detailed electrochemical measurements with synchrotron-based X-ray photoelectron spectroscopy (XPS) depth profiling to determine which pre-passivated electrode (anode or cathode) plays a dominant role in protecting from continuous decomposition of the non-flammable FEMC electrolyte. Furthermore, we investigated the underlying mechanisms by analyzing the surface compositions of pre-passivated electrodes after aging in FEMC, providing critical insights into why this method improves battery performance.

2. Results & discussion

2.1. Galvanostatic cycling performance

Galvanostatic cycling was performed using commercially available NMC622 ($LiNi_{0.6}Mn_{0.2}Co_{0.2}O_2$) and graphite electrodes. Before long-term cycling, a formation cycling protocol was conducted in LP57 (1 M $LiPF_6$ in EC/EMC 3 : 7) with C-rates of C/10 (2 cycles) followed by C/5 (2 cycles). Long-term cycling in the non-flammable 1 M $LiPF_6$ in FEMC electrolyte was carried out at a C/2 rate. Fig. 1a presents the galvanostatic cycling results for FEMC without pre-passivation (red), the benchmark electrolyte LP57 (blue), and FEMC with pre-passivated electrodes (green). The reproducibility of these results is confirmed in Fig. S2 of the SI.

The FEMC electrolyte without pre-passivation exhibits rapid capacity fading within the first few cycles, rendering it unsuitable for long-term battery operation.[7] In contrast, the benchmark carbonate-based electrolyte LP57 demonstrates stable cycling behavior with only minor capacity losses over the first 100 cycles.

At 25 °C, LP57 provides a relatively high ionic conductivity of ~8–9 mS cm^{-1}, whereas fluorinated carbonate solvents such as FEMC exhibit significantly lower conductivities, typically in the range of ~1–5 mS cm^{-1} at comparable salt concentrations. This pronounced difference in ionic

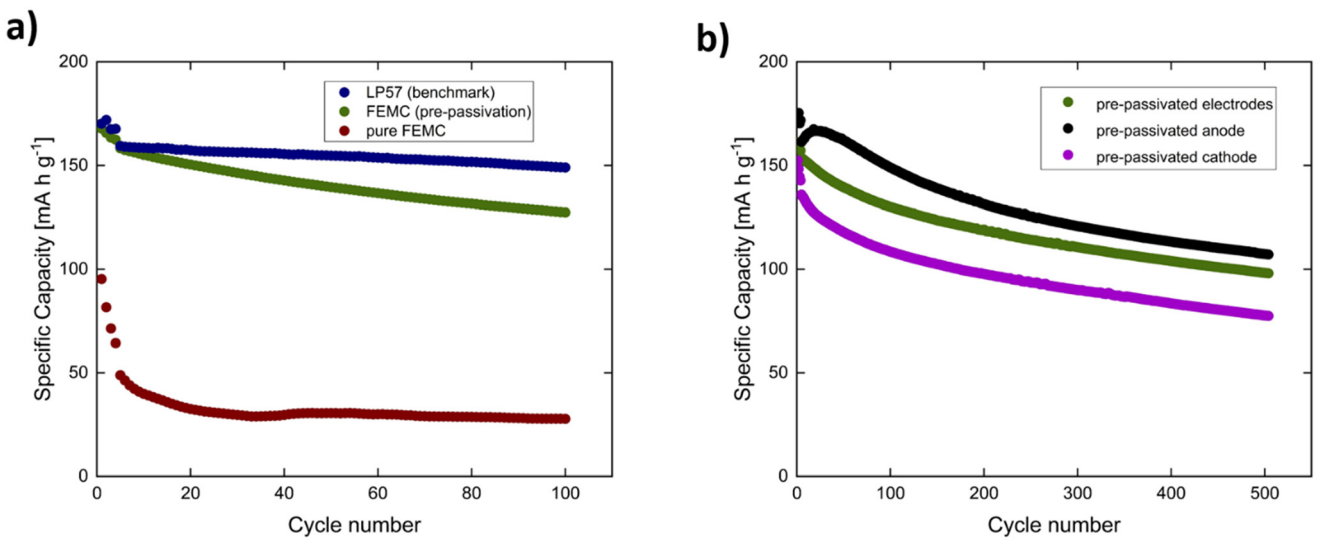

Fig. 1 Galvanostatic cycling performance of NMC622//graphite cells at C/2 rate under various electrolyte and pre-passivation conditions. (a) Comparison of cycling stability using pure FEMC (red), benchmark LP57 (blue), and FEMC following a pre-passivation protocol (green). (b) Influence of selective electrode pre-passivation: cell with only the anode pre-passivated (black), only the cathode pre-passivated (purple), and both electrodes pre-passivated (green), demonstrating the individual and combined effects on long-term cycling.

transport likely contributes, alongside interphase-related effects discussed below, to the inferior cycling behavior observed for FEMC based cells.[5,7,9]

Notably, after pre-passivation of the NMC622 cathode and graphite anode in LP57 and subsequently switching to FEMC, a significant improvement in cycling performance is observed.[8] This shows that pre-passivation is highly effective in enabling stable operation in FEMC. However, the underlying mechanism behind this drastic enhancement remains unclear, particularly regarding which interphase, the SEI on the graphite anode or the CEI on the NMC622 cathode, is primarily responsible for the improved stability.

To address this question, an experiment was conducted to evaluate the impact of pre-passivating each electrode individually, as shown in Fig. 1b. The galvanostatic cycling results compare three cases: (i) both electrodes pre-passivated in LP57 (green), (ii) only the graphite anode pre-passivated while the cathode remains pristine (black), and (iii) only the NMC622 cathode pre-passivated while the anode remains pristine (purple). The reproducibility of these results is confirmed in Fig. S2c and S3 of the SI.

A central outcome of these experiments is that any pre-passivation results in a significant improvement over the pristine/pristine system.[7,8] This is particularly noteworthy for the cathode-only pre-passivated cell, since one might expect that pre-passivating only the cathode would contribute little. Instead, it already provides a clear stabilization effect, which suggests that CEI-derived species may influence interphase formation on the graphite side as well. The most stable performance is observed when only the anode is pre-passivated, while the case where both electrodes are pre-passivated lies between the two cases. These differences are reproducible but not enormous, and should be considered in light of sample size limitations.

The slightly lower capacity observed for the cathode-only case can in part be attributed to a reduced lithium inventory after cathode pre-passivation, where lithium consumed during interphase formation is no longer available to the full cell. Nonetheless, the improvement over the pristine/pristine baseline remains substantial, underscoring that even selective pre-passivation can stabilize FEMC-based cells.[7,8]

From an industrial perspective, this approach could be implemented by pre-passivating the graphite anode in a dedicated electrochemical bath using a three-electrode setup, where the graphite serves as the working electrode and SEI formation is induced *via* controlled formation cycling in a high-conductivity electrolyte such as LP57. Only the graphite anode would need to be pre-passivated, as our results indicate this scenario provides the best performance. The CEI on the cathode could then form *in situ* during subsequent cycling in the FEMC-based electrolyte, simplifying the process and avoiding the need for pre-treatment of both electrodes. This strategy offers a scalable pathway to integrate selective pre-passivation into industrial cell production while maintaining the benefits observed in laboratory testing.

The following sections present a detailed electrochemical analysis to further explore these findings. In particular, we show that differences between the three configurations correspond to distinct electrochemical signatures and interphase chemistries, and we discuss why even cathode-only pre-passivation has a measurable effect on the graphite SEI.

2.2. Deeper electrochemical analysis

Fig. 2a–d presents the specific capacity *versus* voltage plots for the different experiments detailed in Section 2.1. By analyzing these plots, the irreversible capacity loss after the first cycle is clearly visible. Each experiment is displayed from the 1st to the 5th cycle to illustrate the cycling behavior beyond the initial capacity loss.

Irreversible capacity losses after the first cycle are typically associated with interphase formation in batteries, where electrolyte and salt are irreversibly consumed to form both the SEI and CEI layers.[15,16] This process results in reduced capacity and lower coulombic efficiencies during the initial cycles (Fig. 2 and S4). Fig. 2a demonstrates the severe capacity loss observed in pure FEMC without pre-passivated electrodes, where a substantial irreversible capacity loss occurs after the first cycle.[7,8] Furthermore, the formed interphase lacks protective capabilities, leading to rapid capacity fading, with the discharge capacity dropping below 50 mA h g^{-1} after just five cycles.

In contrast, Fig. 2b shows the results for FEMC with pre-passivated electrodes, exhibiting highly stable cycling behavior. The pre-passivation step in LP57 successfully forms a protective and conductive interphase that enables operation in FEMC, as indicated by the minimal irreversible capacity loss after the first cycle. The discharge capacity remains around 155 mA h g^{-1} after five cycles, further supporting this observation.[8]

The improvement in performance is also reflected in the cell resistance, which was tracked *via* the intermittent current interruption (ICI) method, as previously reported by our group.[8] Consistent with these earlier observations, the resistance of pure FEMC cells without pre-passivation is the highest among the three systems, while LP57 with pristine electrodes exhibits the lowest resistance. Pre-passivation of the electrodes in LP57 substantially reduces the cell resistance compared with pristine FEMC cells, although it remains slightly higher than LP57. These differences directly reflect the quality of the formed interphase, as increases in resistance are often associated with detrimental interphase formation.[5,7] The results highlight that pre-passivation not only stabilizes the interphase by protecting the electrolyte from continuous degradation but also improves interfacial conductivity, enabling more efficient lithium transport through the SEI and mitigating the resistive effects that otherwise dominate in pristine FEMC cells.[7,8]

Fig. 2c and d present results for experiments where only one electrode was pre-passivated. In both cases, the

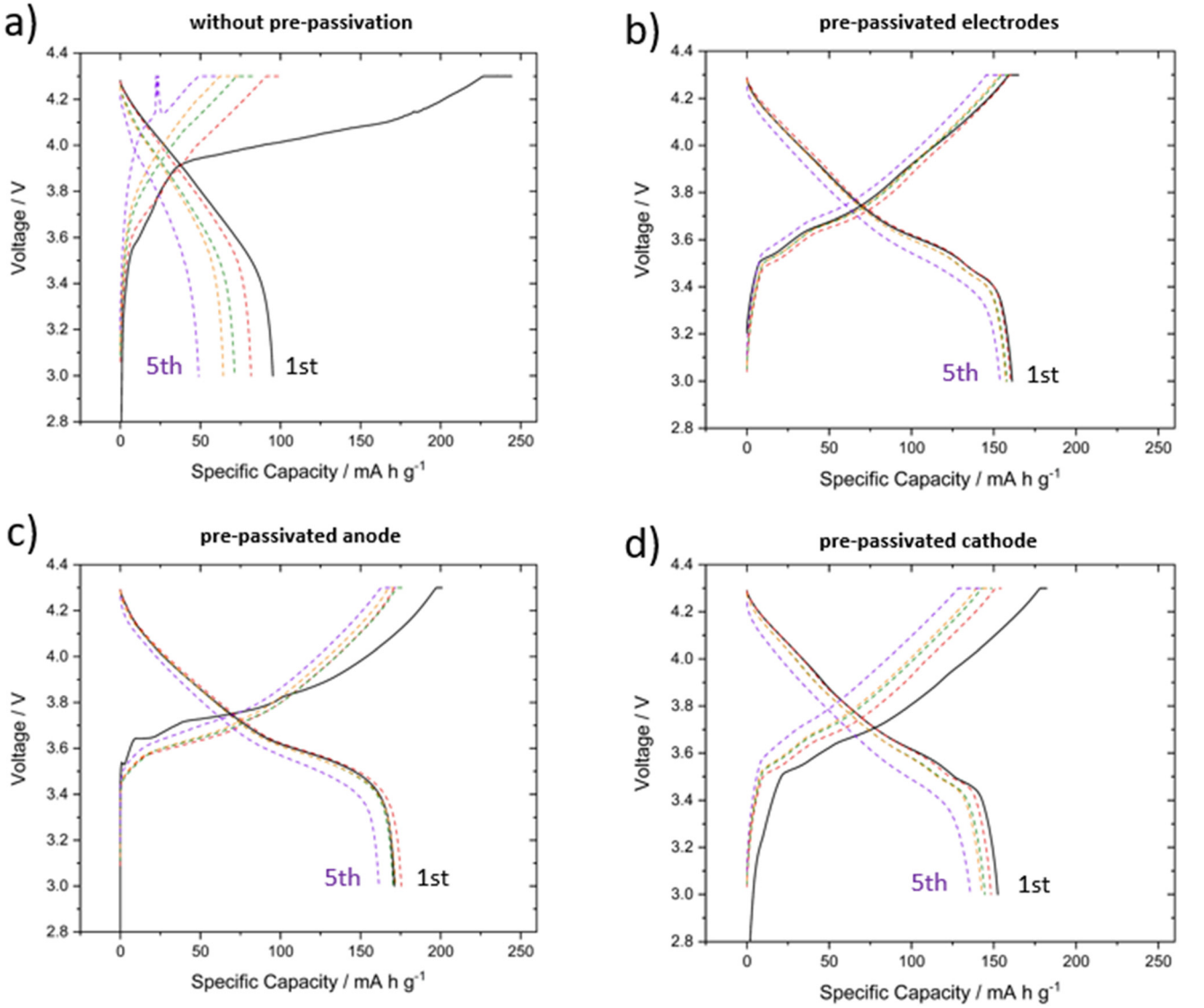

Fig. 2 Specific charge and discharge capacities *vs.* voltage curves for NMC622//graphite cells cycled at C/2 rate under various pre-passivation conditions. (a) FEMC with no pre-passivation; (b) FEMC with both anode and cathode pre-passivated; (c) FEMC with pre-passivated anode and pristine cathode; (d) FEMC with pre-passivated cathode and pristine anode.

first-cycle irreversible capacity loss (~25 mAh g^{-1}) is higher than when both electrodes were pre-passivated, consistent with ongoing electrolyte decomposition at the pristine surface. Importantly, however, both partial pre-passivation strategies still deliver much better stability than the pristine/pristine configuration, highlighting that selective pre-passivation is already sufficient to stabilize FEMC cells.[7]

When only the anode was pre-passivated (Fig. 2c), the cell achieved the highest discharge capacity after the 5th cycle (~160 mAh g^{-1}). When only the cathode was pre-passivated (Fig. 2d), somewhat lower capacity and stability were observed, though still clearly above the pristine baseline. These differences are real and reproducible, but not enormous, and must be interpreted cautiously with respect to statistical significance. Nevertheless, the variations between the three cases correlate with different electrochemical features and interphase compositions.

The slightly reduced capacity of the cathode-only case can be partly explained by lithium inventory effects. During cathode pre-passivation, a fraction of lithium is irreversibly consumed in interphase formation, leaving the cathode lithium-deficient. Since the cathode is the sole lithium source in the full cell, this lowers the available lithium when paired with a pristine anode. The observed ~10–15% lower initial capacity compared to the anode-pre-passivated case is in good agreement with the lithium consumption typically seen during the first formation cycle of pristine full cells.

At the same time, the electrochemical signatures indicate that lithium inventory alone cannot fully account for the observed differences. The dQ/dV profiles (Fig. 3a–c) provide further insight. The anode-only pre-passivated cell (Fig. 3b)

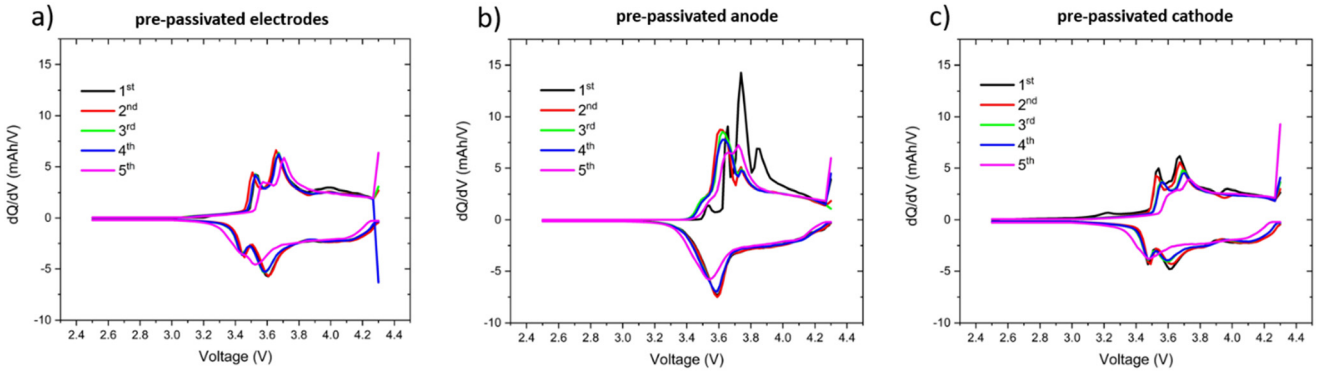

Fig. 3 Differential capacity (d*Q*/d*V*) plots for NMC622//graphite cells cycled at C/2 rate in FEMC under different pre-passivation conditions. (a) FEMC with both anode and cathode pre-passivated; (b) FEMC with pre-passivated anode and pristine cathode; (c) FEMC with pre-passivated cathode and pristine anode.

shows distinct additional peaks between 3.5 and 4.0 V during the first charge, which likely correspond to CEI formation on the pristine cathode. In contrast, the cathode-only and both pre-passivated cases (Fig. 3a and c) exhibit more stable redox behavior from the beginning. These differences suggest that the nature of the interphases, and the sequence in which they form, depends on which electrode is pristine at the start of cycling.[17,18]

Moreover, in the cathode-only pre-passivated configuration, the anode interphase also differs significantly from that of the pristine/pristine cell. This points toward cross-talk effects, where CEI-derived species migrate from the cathode and contribute to SEI formation on the graphite side.[17,18] XPS depth profiling (Section 2.3) supports this interpretation, showing that the SEI in the cathode-pre-passivated system is thinner and more protective than in the pristine/pristine case.[7] While the exact cross-talk mechanism remains a hypothesis, the combined electrochemical and interfacial evidence indicates that it plays a meaningful role in stabilizing the cathode-only pre-passivated cells.

Taken together, these results highlight two main conclusions: (i) pre-passivating either electrode significantly improves cycling stability in FEMC compared to pristine electrodes, and (ii) the differences between the three

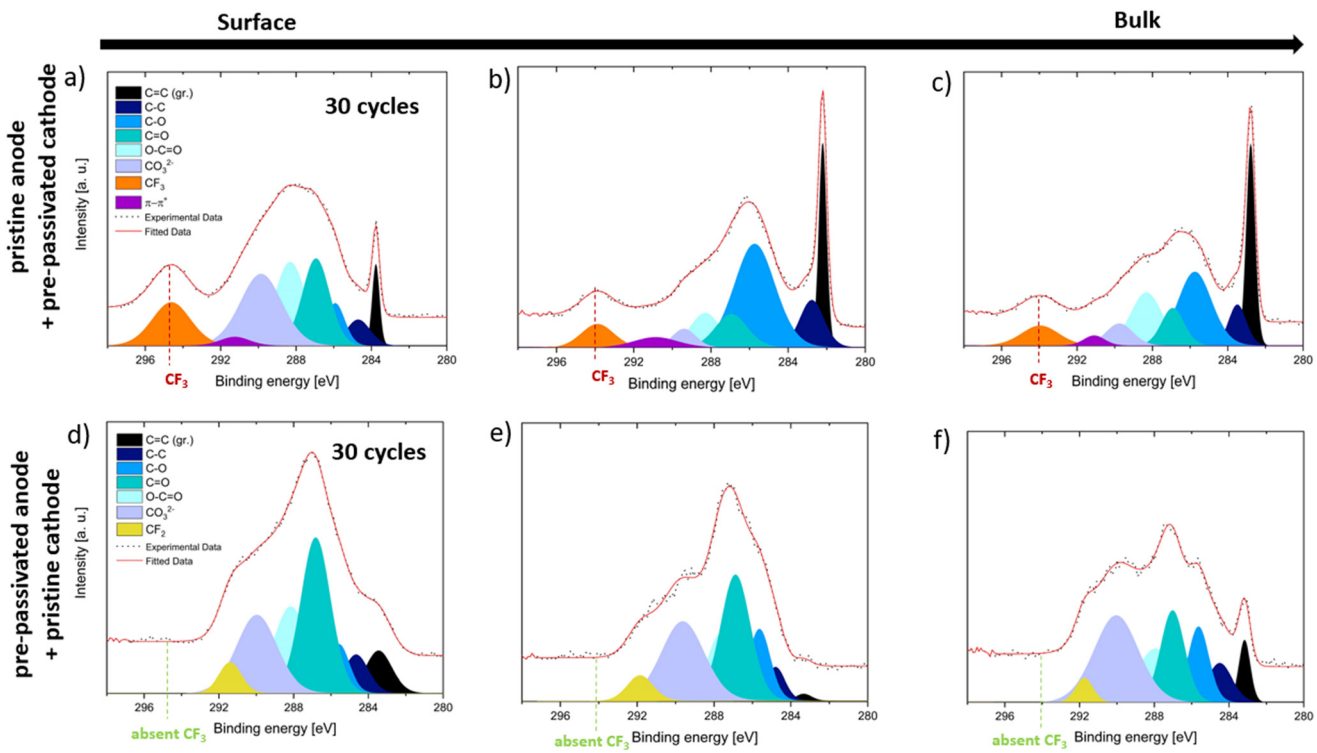

Fig. 4 C 1s XPS spectra acquired at excitation energies of 505 eV (a and d), 2.35 keV (b and e), and 7.05 keV (c and f) showing the SEI composition on graphite electrodes from NMC622//graphite cells aged for 30 cycles at C/2 in FEMC under different pre-passivation protocols: (a–c) cathode pre-passivated, anode pristine; (d–f) anode pre-passivated, cathode pristine.

configurations reflect both lithium inventory effects and distinct interphase chemistries, with possible cross-talk processes linking the cathode and anode.[19–23]

2.3. Interphase chemistry and structure

The C 1s XPS depth profiling data in Fig. 4a–f illustrate the SEI composition on graphite anodes after 30 cycles in FEMC, with panels a–c showing a pristine anode paired with a pre-passivated cathode, and panels d–f showing a pre-passivated anode paired with a pristine cathode. The spectra were collected at increasing photon energies, 505 eV in the soft X-ray regime (Fig. 4a and d), 2.35 keV (Fig. 4b and e; probing depth ~20 nm), and 7.05 keV in the hard X-ray regime (Fig. 4c and f; probing depth ~50 nm) thus enabling compositional analysis from the outermost SEI surface to deeper layers toward the electrode bulk.

All spectra display characteristic carbon species in the 285–292 eV range, corresponding to C–C (285 eV), C–O (286 eV), C═O (287 eV), O–C═O (288 eV), and CO_3^{2-} (290 eV), which are associated with protective and ion-conductive SEI components.[24–27]

A clear difference is observed between the two configurations in terms of SEI thickness and composition. In the pristine anode case (Fig. 4a–c), a strong graphite substrate signal (C═C, 282–284 eV) is still visible even at the lower photon energies, indicating a relatively thin SEI layer. In contrast, in the pre-passivated anode case (Fig. 4d–f), the signals from oxidized carbon species dominate the spectra and persist deeper into the SEI, relative to the underlying graphite signal. This suggests a thicker and more uniformly protective SEI across the probed depths.

Furthermore, a distinct CF_3 peak at ~294 eV serving as a fingerprint of FEMC decomposition is observed only in the pristine anode case (Fig. 4a–c) and is absent in the pre-passivated anode spectra (Fig. 4d–f). This provides direct evidence that anode pre-passivation in a conventional electrolyte such as LP57 prevents FEMC degradation, thereby promoting formation of a more stable and protective SEI layer.

A rough estimation based on the signal attenuation and probing depths suggests the SEI thickness in the pre-passivated case exceeds 20–30 nm.[24–27]

A more detailed analysis of the surface composition under the different pre-passivation protocols is provided in the SI (Fig. S5–S12), which includes additional elemental XPS spectra such as O 1s, F 1s and Li 1s, as well as data for different states of charge and varying cycle numbers. This extended dataset highlights the behavior of both pre-passivated and non-pre-passivated SEI layers during aging in FEMC. In Fig. S5, showing the C 1s XPS spectra corresponding to the experiment where the cathode was pre-passivated and the anode remained pristine, a distinct evolution of the SEI during the first charge between 3.0 V and 4.3 V is observed. The relative decrease in the electrode signal intensity compared to the SEI components suggests significant SEI growth during this phase. However, with continued cycling, a partial dissolution of the SEI becomes apparent, as indicated by the re-emergence of the electrode signal at 1 and 30 cycles.[27–30]

Depth profiling data reveal that under these conditions, the CF_3 signal indicative of FEMC decomposition is initially localized near the SEI surface but becomes increasingly prominent throughout the entire SEI depth after 30 cycles, including at a photon energy of 7.05 keV (~50 nm probing depth). This suggests that the SEI undergoes continuous partial dissolution and reformation during cycling, allowing decomposition products such as CF_3 to penetrate deeper into the SEI structure over time. The persistence and depth distribution of the CF_3 signal indicate that the initially formed SEI is not fully stable and that ongoing FEMC degradation contributes to its evolving composition throughout extended cycling.[31,32]

A complementary dataset is provided in Fig. S6, which presents the C 1s XPS spectra for the experiment where the anode was pre-passivated and the cathode left pristine. In this case, the SEI exhibits a notably more stable and protective behavior. From 4.3 V onward and across all 30 cycles, the SEI contains a consistent presence of protective and conductive carbon–oxygen species.[33,34] Moreover, these beneficial components are distributed throughout the SEI thickness, and no CF_3 signal from FEMC decomposition is detected even at higher photon energies, indicating minimal ongoing electrolyte degradation.[8]

Further insights into the interphase composition are obtained from the O 1s XPS spectra shown in the SI (Fig. S7 and S8), which provide depth-resolved information on oxygen-containing species within the SEI. Fig. S7 corresponds to the experiment where the cathode was pre-passivated and the anode was left pristine. At the beginning of cycling, the SEI is mainly composed of ether-type C–O species (~534 eV) and $LiPOF_x$ compounds (~537 eV), which are typically associated with electrolyte decomposition products.[26,27] After 30 cycles, this composition persists, although depth profiling with photon energies of 2.35 keV and 7.05 keV reveals the appearance of fluorinated organic species (~536 eV) closer to the surface and deeper into the SEI of the electrode. This further suggests ongoing electrolyte decomposition and gradual incorporation of fluorinated compounds into the outer and inner SEI, indicating a less stable interphase.[28,31–33]

In contrast, Fig. S8 shows the O 1s spectra for the experiment in which the anode was pre-passivated. Here, a significantly lower content of organic fluorine species is detected at the lower photon energies of 750 eV and 2.35 keV. This is attributed to SEI formation during pre-passivation in LP57, which has relatively low fluorine content from the $LiPF_6$ salt, compared to FEMC, where both the CF_3 groups in the solvent and the $LiPF_6$ salt result in a much higher fluorine content. The suppression of fluorine-containing species near the surface supports the idea that the pre-passivated anode inhibits continuous FEMC decomposition,

thereby contributing to interphase stability. After 30 cycles, the SEI in this case also contains ether-type C–O species (~534 eV), similar to the pristine anode scenario. However, in addition, inorganic Li_2CO_3 (~532 eV) is observed at 2.35 keV. Li_2CO_3 is known to be a beneficial SEI component, valued for its stability and lithium-ion conductivity, and its presence further supports the formation of a protective and robust SEI during the pre-passivation process.[33,34] The organic fluorine species seen at ~536 eV at the higher photon energy of 7.05 keV likely originate from PF_6^- anion decomposition in the LP57 electrolyte and subsequent reactions with organic fragments during pre-passivation.[32] Since these species are primarily detected deeper in the SEI, closer to the electrode bulk, it suggests that they are remnants of the initial SEI formation and not the result of continuous FEMC degradation.

Interestingly, the experiment involving a pre-passivated cathode and a pristine anode still demonstrates markedly improved cycling performance compared to the system in which both electrodes remain pristine in FEMC. This is consistent with prior studies, which have shown that FEMC alone, when used in NMC622/graphite cells without any pre-passivation, tends to form a thick, unstable interphase with poor protective and conductive characteristics.[7] Despite the anode being left pristine in the experiment with a pre-passivated cathode, the SEI formed on the graphite surface appears significantly different from that in the pristine FEMC cell as reported previously.[7] This suggests a potential influence of the cathode CEI on the anode SEI *via* electrolyte-mediated cross-talk.

It is plausible that species from the CEI, formed during LP57 pre-passivation, dissolve into the electrolyte during cycling and subsequently deposit onto the anode surface, thereby modifying the SEI structure and composition.[35–37] This hypothesis is supported by comparative analysis of the C 1s XPS spectra shown in Fig. 4a–c and S5, as well as previously reported data for pristine NMC622/graphite cells in FEMC.[7] While FEMC continues to decompose at the anode surface in this scenario, the influence of the preformed CEI appears to limit this degradation, resulting in a thinner and more protective SEI after 30 cycles. The thinner SEI is corroborated by the enhanced visibility of the graphite electrode signal, suggesting reduced interphase thickness when influenced by CEI-derived species from the cathode.

Nonetheless, the overall electrochemical performance of this configuration remains inferior to that of the system in which the anode is pre-passivated or both electrodes are pre-passivated. This highlights that the principal challenge for next-generation electrolytes like FEMC lies in stabilizing the anode interphase.[7,8,38] The results clearly indicate that when only the cathode is pre-passivated and the anode is left pristine, FEMC continues to undergo substantial decomposition at the anode, resulting in capacity loss. Conversely, pre-passivating the anode in LP57 leads to the formation of a robust SEI that effectively mitigates FEMC degradation, stabilizing the interface and minimizing

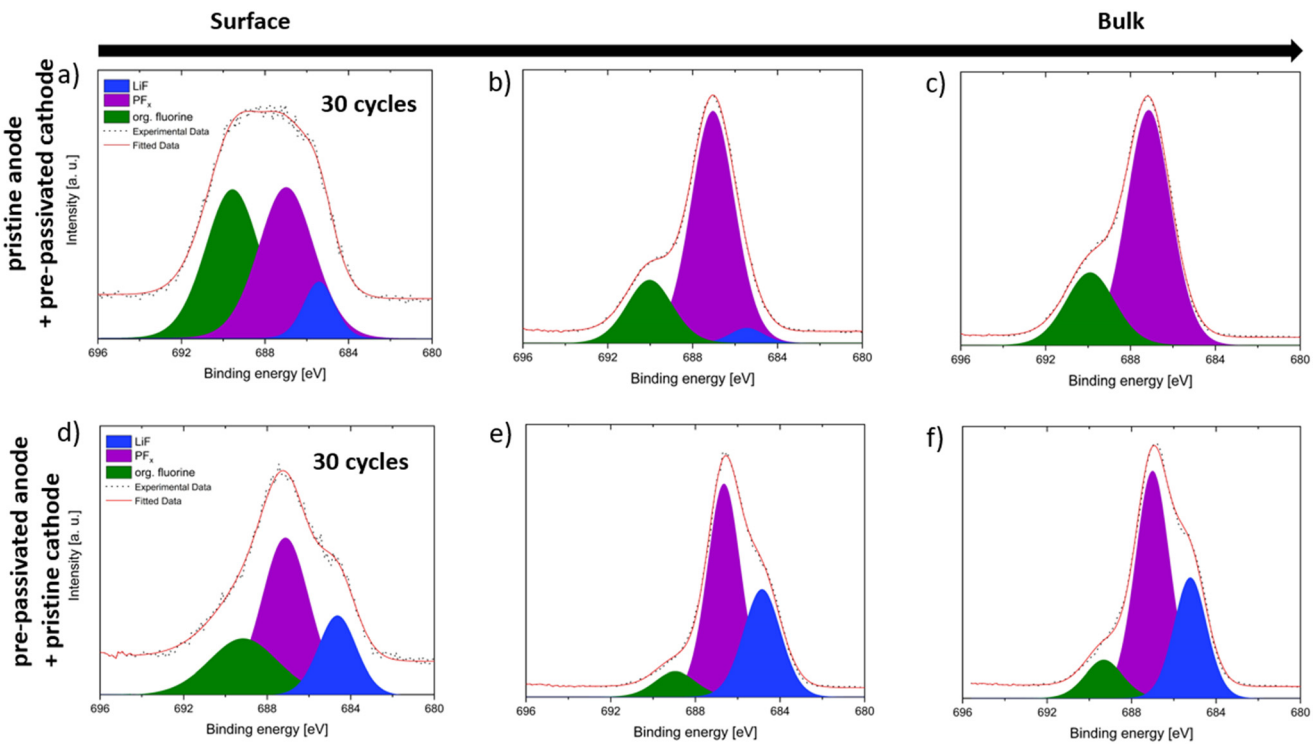

Fig. 5 F 1s XPS spectra acquired at excitation energies of 505 eV (a and d), 2.35 keV (b and e), and 7.05 keV (c and f), showing the SEI composition on graphite electrodes from NMC622//graphite cells aged for 30 cycles at C/2 in FEMC under different pre-passivation protocols: (a–c) cathode pre-passivated, anode pristine; (d–f) anode pre-passivated, cathode pristine.

additional SEI growth. These findings highlight the critical role of pre-passivation in improving SEI stability. In particular, FEMC proves to be a highly effective model electrolyte for probing interfacial reactions due to its distinct CF_3 decomposition marker, which can be clearly tracked using XPS.[8] This enables detailed evaluation of SEI stability and electrolyte decomposition behavior under different pre-passivation conditions.

Further insights into these interphase properties are obtained from the F 1s XPS spectra in Fig. 5a–f, S9 and S10, which provide depth profiles of fluorine containing species from the electrode surface to the bulk with panels a–c in Fig. 5 showing a pristine anode paired with a pre-passivated cathode, and panels d–f showing a pre-passivated anode paired with a pristine cathode.

The F 1s spectra reveal that, when the anode is left pristine, a higher concentration of organic fluorine species (C–F_x, ~690 eV) is detected throughout the entire SEI thickness compared to the case where the anode is pre-passivated. In the latter scenario, the amount of organic fluorine is significantly reduced, suggesting that pre-passivation suppresses the formation of organic fluorinated decomposition products, likely through early SEI stabilization.[27] In contrast, the LiF peak (~685 eV), a stable and beneficial inorganic SEI component known to improve SEI robustness, is significantly more pronounced when the anode is pre-passivated.[39,40] This suggests that pre-passivation promotes the formation and retention of a LiF-rich SEI, which is generally associated with favorable long-term stability. Additionally, inorganic PF_x species (~688 eV), originating from the reduction of the PF_6^- anion, are observed in both experimental cases.[41]

These conclusions are further supported by the Li 1s spectra presented in the SI (Fig. S11 and S12), which are consistent with the trends observed in the F 1s region.[39–41] While it is difficult to unambiguously separate different species in Li 1s due to its ionic nature, a signal at ~57 eV, tentatively attributed to LiF, shows distinct differences depending on the pre-passivation conditions. In the case where the anode is left pristine and only the cathode is pre-passivated (Fig. S11), this Li 1s signal becomes less prominent across the SEI depth after 30 cycles of aging in FEMC, suggesting a loss of LiF over extended cycling. Although LiF-related species can be detected in the Li 1s region before aging, they diminish over time and are no longer clearly visible after 30 cycles. In contrast, when the anode is pre-passivated (Fig. S12), the corresponding Li 1s signal remains more intense and persistent throughout the SEI even after 30 cycles. These observations align with the F 1s spectra, where the presence of LiF is more clearly resolved, and together they indicate that anode pre-passivation promotes the formation of a LiF-rich SEI that is chemically and structurally more stable under extended cycling. As LiF is widely recognized as a beneficial SEI component contributing to mechanical integrity,[39] its sustained presence points to a robust and passivating interphase, whereas the absence of pre-passivation results in a more organic, less stable SEI prone to continuous decomposition and restructuring.[40]

The C 1s XPS spectra of the CEI formed on NMC622 surfaces, as presented in Fig. 6a and b, provide insights into how the FEMC and LP57 electrolytes influence CEI formation after 30 cycles of aging in FEMC. Fig. 6a corresponds to the experiment in which the anode was left pristine and the cathode was pre-passivated, while Fig. 6b depicts the condition where the anode was pre-passivated and the cathode was left pristine. Comparing these two cases allows for a direct assessment of how pre-passivation in LP57 affects the resulting CEI when the subsequent long-term cycling is carried out in FEMC.

In Fig. 6a, the CEI formed on the pre-passivated cathode from the LP57 electrolyte displays characteristic carbonaceous species at binding energies of 285 eV (C–C),

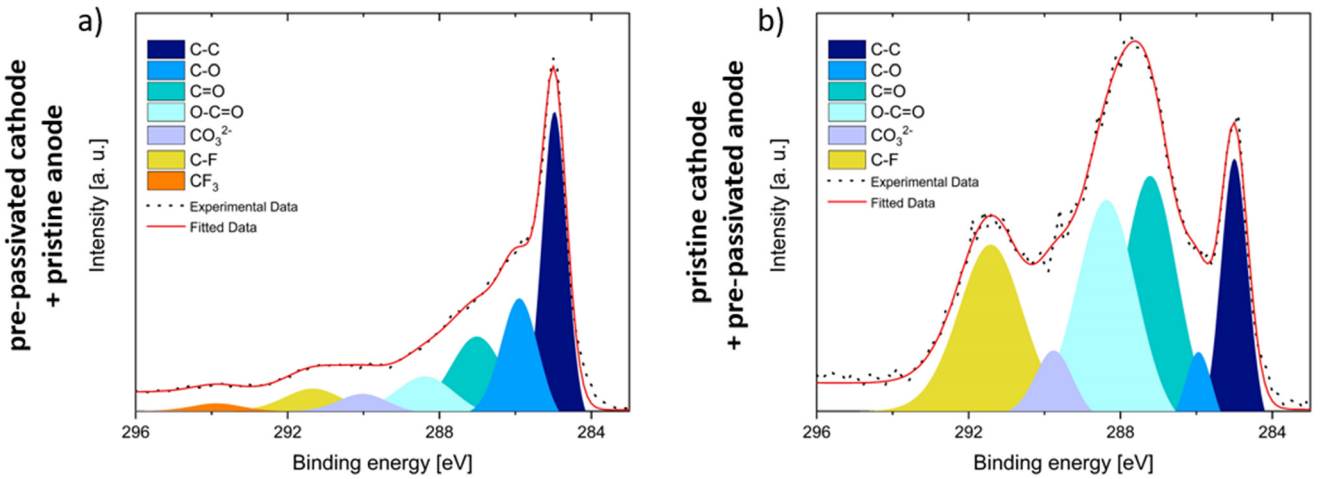

Fig. 6 C 1s XPS spectra acquired at an excitation energy of 2.35 keV showing the CEI composition on NMC622 electrodes from NMC622//graphite cells aged for 30 cycles at C/2 in FEMC under different pre-passivation protocols: (a) cathode pre-passivated, anode pristine and (b) anode pre-passivated, cathode pristine.

286 eV (C–O), 287 eV (C═O), 288 eV (O–C═O), and 290 eV (CO_3^{2-}). These species are commonly associated with the decomposition products of carbonate-based solvents, and they are frequently observed within the SEI formed on anode surfaces.[25–27,42] In addition to these signals, a small amount of CF_3 and C–F_x species is also present, likely originating from the decomposition of FEMC during long-term cycling.

This observation suggests that although a CEI formed by LP57 pre-passivation is present, it is not fully protective, as FEMC continues to decompose and contributes to the interphase structure during aging.

In contrast, the CEI formed on the pristine cathode (Fig. 6b), where no LP57 pre-passivation was employed, exhibits a higher intensity for some oxidized carbon species, specifically those at 287 eV (C═O), 288 eV (O–C═O), and 290 eV (CO_3^{2-}). These species are typically linked to protective and conductive interphase characteristics, implying that the CEI formed directly from FEMC reduction may offer better passivation compared to one initially formed by LP57.[43]

Additionally, a higher amount of C–F_x species is observed in this case, which is expected since FEMC, as a partially fluorinated solvent, contributes directly to CEI formation through its decomposition.[44]

Relating these findings to the electrochemical cycling results, a consistent picture emerges. The experiment in which only the anode is pre-passivated shows the best cycling performance, which can be rationalized by the complementary interphase properties formed under these conditions. The anode SEI, pre-formed in LP57, is more effective in passivating the surface and preventing further decomposition of FEMC, thus enhancing overall stability.[3,5,29,45] On the other hand, the CEI formed directly from FEMC on the pristine cathode exhibits a richer composition of beneficial oxidized carbon species, which likely contributes to improved charge transport and structural stability.[18,37,43]

In summary, the SEI formed on the anode benefits significantly from LP57 pre-passivation, whereas the CEI on the cathode appears to form more favorable properties directly from FEMC. This asymmetry in interphase formation helps explain why selectively pre-passivation only the anode leads to the most stable and high-performing cycling behavior in FEMC-based cells.

3. Conclusions

This study systematically investigated the impact of electrode pre-passivation on the cycling performance of the non-flammable electrolyte FEMC. Using electrochemical measurements and synchrotron-based XPS, we demonstrated that both a pre-formed SEI and a pre-formed CEI significantly improve performance, with the SEI showing a slight advantage in stabilizing cycling. Our results show that pre-passivating the anode, while keeping the cathode pristine, yields the most consistent improvement in cycling stability. XPS data reveal that the SEI formed in conventional LP57 electrolyte offers superior protection compared to SEIs formed directly in FEMC, whereas FEMC outperforms LP57 in forming a more stable CEI, as shown by CEI composition comparisons. We also observed that cathode pre-passivation indirectly benefits anode SEI formation, likely due to electrode cross-talk, with a CEI formed in LP57 positively influencing the subsequent SEI in FEMC-aged cells. Notably, the absence of CF_3 degradation signals in XPS confirms that pre-passivation of the anode with LP57 effectively protects FEMC from further breakdown.

These findings highlight that interphase engineering on both electrodes can stabilize advanced electrolytes like FEMC, with the formation of a pre-passivated SEI providing the most pronounced benefit. Future studies could investigate how pre-passivation conditions such as C-rate, temperature, or additive inclusion affect interphase properties. This strategy may also be applicable to other non-flammable electrolytes and sodium-ion battery systems, where interphase stability remains a major challenge.

4. Material and methods

4.1. Preparation of materials

Commercially prepared electrode sheets were used in this study: NMC622 ($LiNi_{0.6}Mn_{0.2}Co_{0.2}O_2$) cathodes coated on 20 μm aluminum foil with an areal capacity of 2.0 ± 0.1 mAh cm^{-2} and a thickness of 100 ± 4 μm, and graphite anodes coated on 10 μm copper foil with an areal capacity of 2.4 ± 0.1 mAh cm^{-2} and a thickness of 100 ± 5 μm, both obtained from CustomCells (Itzehoe, Germany). Reported thickness values correspond to the total coating layer on one side of the current collector, excluding the metal foil. The electrodes were single-side coated, with a calculated porosity of 44 ± 4% for the graphite anodes and 39 ± 4% for the NMC622 cathodes, based on electrode density and formulation. Discs 13 mm in diameter were punched from these sheets and dried under vacuum at 120 °C for 12 hours prior to use. The electrodes included standard conductive carbon and binder components. Active material loading was approximately 93.5% for the cathode and 95.0% for the anode, with an N/P ratio of 1.2 to ensure lithium balance. All handling and assembly steps were performed in an argon-filled glove box (MBraun) where oxygen and moisture levels were maintained below 1 ppm to avoid moisture and air contamination. Pouch cells were assembled for the pre-passivation step using aluminum-laminated film and gently clamped between flat plates, resulting in low applied stack pressure. A Celgard® 2400 polypropylene membrane was used as the separator. Coin-type 2025 cells were assembled for long-term cycling using standard coin cell hardware, providing the typical spring-defined stack pressure. In both pouch and coin cells, 35 μL of electrolyte was added per electrode, corresponding to 35 μL per side of the separator. The LP57 electrolyte (1 M $LiPF_6$ in EC : EMC, 3 : 7 vol%) was sourced from Solvionic and used as received. The FEMC-based electrolyte was prepared inside the glove box by dissolving 1 M $LiPF_6$ (99.99%, Sigma

Aldrich) in commercial-grade FEMC solvent (98.0%, TCI Chemicals). The $LiPF_6$ salt was vacuum-dried at 70 °C while the FEMC solvent was dried over activated molecular sieves for three days and subsequently filtered through a dry syringe filter before electrolyte preparation. All electrochemical cycling was conducted at room temperature (25 °C).

4.2. Electrochemical measurements

Electrode pre-passivation was performed by assembling full cells (NMC622//graphite) and cycling them twice at C/10 (corresponding to an areal current density of ~0.20 mA cm^{-2}, based on a cathode areal capacity of 2.0 mAh cm^{-2}; absolute current ~0.265 mA for a 13 mm electrode) and twice at C/5 (~0.40 mA cm^{-2}; absolute current ~0.53 mA) between 3.0 and 4.3 V. These cycles were carried out in LP57 electrolyte, following a standard preconditioning protocol. After cycling, the electrodes were extracted inside the glove box, rinsed with 50 μL of FEMC to remove residual LP57, air-dried within the box for about 5 minutes, and then reassembled into new cells using 1 M $LiPF_6$ in FEMC as the operating electrolyte.

While complete removal of residual LP57 cannot be guaranteed, control experiments indicate that residual LP57 components are minimal and do not significantly affect subsequent FEMC cycling performance (Fig. S13). The reproducibility of these results is confirmed in Fig. S14.

Galvanostatic cycling was conducted using a constant current–constant voltage (CC–CV) protocol. Cells were charged at C/2 (~1.0 mA cm^{-2} areal current density; absolute current ~1.325 mA) to 4.3 V, followed by a voltage hold until the current dropped to one-tenth of the initial value. Discharge was performed at constant current down to 3.0 V. All cycling tests were conducted using Neware battery testing systems.

Reproducibility of the galvanostatic cycling results was confirmed using at least two independent cells (Fig. S2, S3 and S14). Variations are discussed qualitatively; error bars are not shown due to the limited sample size and cell-to-cell heterogeneity.

4.3. X-ray photoelectron spectroscopy

To prepare samples for X-ray photoelectron spectroscopy (XPS), cells were first charged to the target voltage using a C/10 rate, with the charge process halted precisely once the designated voltage was achieved. Cells intended for analysis after 5 and 30 cycles underwent an initial two cycles at C/10, followed by four and twenty-nine additional cycles at C/2, respectively. After cycling, the cells were carefully disassembled inside an argon-filled glove box. Electrodes were gently rinsed with 50 μL of FEMC to remove residual electrolyte, then dried at room temperature under vacuum for two hours.

The washed electrodes were mounted on copper sample holders using conductive carbon tape and subsequently sealed in vacuum-compatible containers for transport. Transfer between the glovebox and the synchrotron beamline was conducted using a portable vacuum suitcase to prevent atmospheric exposure. XPS data acquisition was carried out at beamline I09 of the Diamond Light Source (Oxfordshire, UK).

For soft X-ray photoemission, photon energies were adjusted to yield a uniform electron kinetic energy of 200 eV for the acquisition of F 1s, O 1s, C 1s, and Li 1s spectra. These soft X-ray were generated using a collimated beam and monochromatized with a plane-grating monochromator. Spectra were recorded at a pass energy of 50 eV. In the case of hard X-ray photoelectron spectroscopy (HAXPES), photon energies of 2350 eV and 7050 eV were employed, selected using a Si(111) double-crystal monochromator, and recorded with a 200 eV pass energy. All spectra were measured using a Scienta EW4000 high-voltage hemispherical analyzer.

The probing depth, defined as three times the inelastic mean free path (3× IMFP) of electrons, was estimated using the TPP-2M predictive model with parameters suited for low-density polymeric materials, such as polyethylene, representative of SEI-type environments (based on the NIST database).[46,47] Data processing and spectral deconvolution were carried out using CasaXPS software. Binding energies were calibrated using the CF_3 peak at 294 eV, which is part of the SEI in the C 1s spectra, whenever possible. When this was not feasible, the C–C/C–H signal at 285 eV was used as the reference instead. Peak fitting employed a mixed Gaussian–Lorentzian (30/70) line shape combined with a Shirley background.

Due to differences in relative sensitivity factors (RSFs) and probing depths, absolute peak intensities are not directly compared between different photon energies. Instead, trends in component distribution across SEI depths are analyzed. The XPS spectra reflect the average signal from a relatively large beam spot, measured using the I09 beamline optics. A defocused beam resulting in an estimated spot size at the sample of approximately 300 μm in the horizontal direction and up to 1 mm in the vertical direction was used. Both configurations inherently integrate over local heterogeneities, providing a representative measurement of the SEI chemistry across the probed area. Statistical mean and SD are not reported due to intrinsic sample heterogeneity and differential charging effects, in agreement with standard practice for spectroscopic analysis of SEI layers.

Author contributions

Lasse Dettmann: methodology, formal analysis, investigation, writing – original draft preparation, writing – review and editing, visualization. Florian Gebert: methodology, formal analysis, investigation. Andrew J. Naylor: conceptualization, methodology, formal analysis, investigation, resources, writing – review & editing, supervision, project administration, funding acquisition.

Conflicts of interest

There are no conflicts to declare.

Data availability

Data for this article, including electrochemical testing data and data from X-ray photoelectron spectroscopy measurements, are available at figshare at https://doi.org/10.6084/m9.figshare.30655691.

Supplementary information (SI) is available, providing flammability test results, and data from electrochemical testing and X-ray photoelectron spectroscopy measurements. See DOI: https://doi.org/10.1039/d5lf00364d.

Acknowledgements

The authors would like to acknowledge the financial support by the Swedish Energy Agency *via* project no. P2021-90019 and P2022-00045 and STandUP for Energy. We acknowledge Diamond Light Source for time on beamline I09 under proposal SI31857. Dr Tien-Lin Lee, Dr Pardeep Thakur Kumar and Dr Deepnarayan Biswas at beamline I09 are thanked for their assistance. The authors thank Maria Hahlin and Habtom Desta Asfaw for valuable discussions related to this work.

References

1 H. Adenusi, G. A. Chass, S. Passerini, K. V. Tian and G. Chen, Lithium Batteries and the Solid Electrolyte Interphase(SEI)—Progress and Outlook, *Adv. Energy Mater.*, 2023, **13**, 2203307.
2 A. Wang, S. Kadam, H. Li, S. Shi and Y. Qi, Review on modeling of the anode solid electrolyte interphase (SEI) for lithium-ion batteries, *npj Comput. Mater.*, 2018, **4**, 15.
3 E. Peled and S. Menkin, Review—SEI: Past, Present and Future, *J. Electrochem. Soc.*, 2017, **164**, A1703–A1719.
4 S. K. Heiskanen, J. Kim and B. L. Lucht, Generation and Evolutionof the Solid Electrolyte Interphase of Lithium-Ion Batteries, *Joule*, 2019, **3**, 2322–2333.
5 K. Xu and A. Von Cresce, Interfacing electrolytes with electrodes in Li ion batteries, *J. Mater. Chem.*, 2011, **21**, 9849–9864.
6 S. Hess, M. W. Mehrens and M. Wachtler, Flammability of Li-Ion Battery Electrolytes: Flash Point and Self-Extinguishing Time Measurements, *J. Electrochem. Soc.*, 2015, **162**, A3084.
7 F. Gebert, N. Gogoi, D. P. Siriwardena and A. J. Naylor, The Origin of Rapid Capacity Loss in 1,1,1-Trifluoroethyl Methyl Carbonate – Based Lithium-Ion Battery Electrolytes, *Adv. Mater. Interfaces*, 2024, **11**, 2400534.
8 M. Longhini, F. Gebert, F. Conti and A. J. Naylor, Enabling a non-flammable methyl(2,2,2-trifluoroethyl) carbonate electrolyte in NMC622–graphite Li-ion cells by electrode pre-passivation, *Energy Adv.*, 2024, **3**, 1087.
9 R. Gond, W. van Ekeren, R. Mogensen, A. J. Naylor and R. Younesi, Non-flammable liquid electrolytes for safe batteries, *Mater. Horiz.*, 2021, **8**, 2913.
10 Y. Lei, K. Wang, S. Jiang, X. Xu, J. Zheng, J. Yin and Y. Gao, Recent Progress on Multifunctional Electrolyte Additives for High-Energy-Density Li Batteries – A Review, *ChemElectroChem*, 2024, **11**, e202300702.
11 G. J. Chung, J. Han and S.-W. Song, Fire-Preventing $LiPF_6$ and Ethylene Carbonate-Based Organic Liquid Electrolyte System for Safer and Outperforming Lithium-Ion Batteries, *ACS Appl. Mater. Interfaces*, 2020, **12**, 42868–42879.
12 J. Jung, H. J. Hah, T. J. Lee, J. G. Lee, J. B. Lee, J. Kim, J. Soon, J. H. Ryu, J. J. Kim and S. M. Oh, Effect of Pre-Cycling Rate on the Passivating Ability of Surface Films on $Li_4Ti_5O_{12}$ Electrodes, *J. Electrochem. Sci. Technol.*, 2017, **8**, 15–24.
13 S. Choi, G. Jung, J. E. Kim, T. Y. Kim and K. S. Suh, Lithium intercalated graphite with preformed passivation layer as superior anode for Lithium ion batteries, *Appl. Surf. Sci.*, 2018, **455**, 367–372.
14 Y. Yu, Z. Yang, Y. Liu and J. Xie, Achieving SEI preformed graphite in flow cell to mitigate initial lithium loss, *Carbon*, 2022, **196**, 589–595.
15 Y. X. Lin, Z. Liu, K. Leung, L. Q. Chen, P. Lu and Y. Qi, Connecting the irreversible capacity loss in Li-ion batteries with the electronic insulating properties of solid electrolyte interphase (SEI) components, *J. Power Sources*, 2016, **309**, 221–230.
16 D. Rehnlund, Z. Wang and L. Nyholm, Lithium-Diffusion Induced Capacity Losses in Lithium-Based Batteries, *Adv. Mater.*, 2022, **34**, 2108827.
17 S. Fang, D. Jackson, M. L. Dreibelbis and T. F. Kuech, Anode-originated SEI migration contributes to formation of cathode-electrolyte interphase layer, *J. Power Sources*, 2018, **373**, 184–192.
18 Y. He, Z. Chen and Y. Zhang, Strategies for improving cathode electrolyte interphase in high-performance dual-ion batteries, *iScience*, 2024, **27**, 110491.
19 X. Lin, Y. Chen, Y. Fu, F. Zeng, Y. Kuai, J. Lin, J. He, L. Xing and W. Li, Fluorinated Thiophene-Based Electrolyte Additives Enable a Robust Cathode Electrolyte Interphase with Conformal Homogeneity for a High-Voltage $LiNi_{0.8}Co_{0.15}Al_{0.05}O_2$ Cathode, *J. Phys. Chem. C*, 2024, **128**, 4988–4996.
20 L. Di, C. Yufang, S. Weiwei, X. Wei, Y. Shuaiyu, L. Shiqiang, Z. Lanlan, Z. Yanshuang, Y. Tianyan, X. Peitao and Z. Chunman, Cathode Electrolyte Interface Engineering by Gradient Fluorination for High-Performance Lithium Rich Cathode, *Adv. Energy Mater.*, 2023, **13**, 2301765.
21 J. Xu, Critical Review on cathode–electrolyte Interphase Toward High-Voltage Cathodes for Li-Ion Batteries, *Nano-Micro Lett.*, 2022, **14**, 1–22.
22 T. Li, X. Q. Zhang, P. Shi and Q. Zhang, Fluorinated Solid-Electrolyte Interphase in High-Voltage Lithium Metal Batteries, *Joule*, 2019, **3**, 2647–2661.
23 H. Wang, X. Li, F. Li, X. Liu, S. Yang and J. Ma, Formation and modification of cathode electrolyte interphase: A mini review, *Electrochem. Commun.*, 2021, **122**, 106870.
24 I. Weber, B. Wang, C. Bodirsky, M. Chakraborty, M. Wachtler, T. Diemant, J. Schnaidt and R. J. Behm, Model Studies on Solid Electrolyte Interphase Formation on Graphite Electrodes in Ethylene Carbonate and Dimethyl Carbonate II: Graphite Powder Electrodes, *ChemElectroChem*, 2020, **7**, 4794–4809.

25 B. Ng, E. Faegh, S. Lateef, S. G. Karakalos and W. E. Mustain, Structure and chemistry of the solid electrolyte interphase (SEI) on a high capacity conversionbased anode: NiO, *J. Mater. Chem. A*, 2021, **9**, 523–537.
26 I. Källquist, R. Le Ruyet, H. Liu, R. Mogensen, M.-T. Lee, K. Edström and A. J. Naylor, Advances in studying interfacial reactions in rechargeable batteries by photoelectron spectroscopy, *J. Mater. Chem. A*, 2022, **10**, 19466–19505.
27 R. Azmi, F. Lindgren, K. Stokes-Rodriguez, M. Buga, C. Ungureanu, T. Gouveia, I. Christensen, S. Pal, A. Vlad, A. Ladam, K. Edström and M. Hahlin, An XPS Study of Electrolytes for Li-Ion Batteries in Full Cell LNMO vs Si/Graphite, *ACS Appl. Mater. Interfaces*, 2024, **16**, 34266–34280.
28 H. Bryngelsson, M. Stjerndahl, T. Gustafsson and K. Edström, How dynamic is the SEI?, *J. Power Sources*, 2007, **174**, 970–975.
29 E. W. C. Spotte-Smith, R. L. Kam, D. Barter, X. Xie, T. Hou, S. Dwaraknath, S. M. Blau and K. A. Persson, Toward a Mechanistic Model of Solid− Electrolyte Interphase Formation and Evolution in Lithium-Ion Batteries, *ACS Energy Lett.*, 2022, **7**, 1446–1453.
30 N. Takenaka, A. Bouibes, Y. Yamada, M. Nagaoka and A. Yamada, Frontiers in Theoretical Analysis of Solid Electrolyte Interphase Formation Mechanism, *Adv. Mater.*, 2021, **33**, 2100574.
31 P. Sayavong, W. Zhang, S. T. Oyakhire, D. T. Boyle, Y. Chen, S. C. Kim, R. A. Vilá, S. E. Holmes, M. S. Kim, S. F. Bent, Z. Bao and Y. Cui, Dissolution of the Solid Electrolyte Interphase and Its Effects on Lithium Metal Anode Cyclability, *J. Am. Chem. Soc.*, 2023, **145**, 12342–12350.
32 B. S. Parimalam, A. D. MacIntosh, R. Kadam and B. L. Lucht, Decomposition Reactions of Anode Solid Electrolyte Interphase (SEI) Components with $LiPF_6$, *J. Phys. Chem. C*, 2017, **121**, 22733–22738.
33 S. J. An, J. Li, C. Daniel, D. Mohanty, S. Nagpure and D. L. Wood III, The state of understanding of the lithium-ion-battery graphite solid electrolyte interphase (SEI) and its relationship to formation cycling, *Carbon*, 2016, **105**, 52–76.
34 M. D. Bouguern and A. K. M R, The critical role of interfaces in advanced Li-ion battery technology: A comprehensive review, *J. Power Sources*, 2024, **623**, 235457.
35 T. Kim, L. K. Ono and Y. Qi, Understanding the active formation of a cathode–electrolyte interphase (CEI) layer with energy level band bending for lithium-ion batteries, *J. Mater. Chem. A*, 2023, **11**, 221–231.
36 Q. Li, Y. Wang, X. Wang, X. Sun, J. N. Zhang, X. Yu and H. Li, Investigations on the Fundamental Process of Cathode Electrolyte Interphase Formation and Evolution of High-Voltage Cathodes, *ACS Appl. Mater. Interfaces*, 2020, **12**, 2319–2326.
37 N. Zhang, B. Wang, F. Jin, Y. Chen, Y. Jiang, C. Bao, J. Tian, J. Wang, R. Xu, Y. Li, Q. Lv, H. Ren, D. Wang, H. Liu, S. Dou and X. Hong, Modified cathode-electrolyte interphase toward high-performance batteries, *Cell Rep. Phys. Sci.*, 2022, **3**, 101197.
38 X. Cao, Y. Xu, L. Zhang, M. H. Engelhard, L. Zhong, X. Ren, H. Jia, B. Liu, C. Niu, B. E. Matthews, H. Wu, B. W. Arey, C. Wang, J. G. Zhang and W. Xu, Nonflammable Electrolytes for Lithium Ion Batteries Enabled by Ultraconformal Passivation Interphases, *ACS Energy Lett.*, 2019, **4**, 2529–2534.
39 G. G. Serbessa, B. W. Taklu, Y. Nikodimos, N. T. Temesgen, Z. B. Muche, S. K. Merso, T. I. Yeh, Y. J. Liu, W. S. Liao, C. H. Wang, S. H. Wu, W. N. Su, C. C. Yang and B. J. Hwang, Boosting the Interfacial Stability of the Li_6PS_5Cl Electrolyte with a Li Anode via In Situ Formation of a LiF-Rich SEI Layer and a Ductile Sulfide Composite Solid Electrolyte, *ACS Appl. Mater. Interfaces*, 2024, **16**, 10832–10844.
40 D. Rakov, M. Hasanpoor, A. Baskin, J. W. Lawson, F. Chen, P. V. Cherepanov, A. N. Simonov, P. C. Howlett and M. Forsyth, Stable and Efficient Lithium Metal Anode Cycling through Understanding the Effects of Electrolyte Composition and Electrode Preconditioning, *Chem. Mater.*, 2022, **34**, 165–177.
41 B. S. Parimalam and B. L. Lucht, Reduction Reactions of Electrolyte Salts for Lithium Ion Batteries: $LiPF_6$, $LiBF_4$, LiDFOB, LiBOB, and LiTFSI, *J. Electrochem. Soc.*, 2018, **165**, A251–A255.
42 R. Stockhausen, L. Gehrlein, M. Mueller, T. Bergfeldt, A. Hofmann, F. J. Mueller, J. Maibach, H. Ehrenberg and A. Smith, Investigating the dominant decomposition mechanisms in lithium-ion battery cells responsible for capacity loss in different stages of electrochemical aging, *J. Power Sources*, 2022, **543**, 231842.
43 Z. Zhang, J. Yang, W. Huang, H. Wang, W. Zhou, Y. Li, Y. Li, J. Xu, W. Huang, W. Chiu and Y. Cui, Cathode-Electrolyte Interphase in Lithium Batteries Revealed by Cryogenic Electron Microscopy, *Matter*, 2021, **4**, 302–312.
44 R. Wang, H. Wang, H. Zhao, M. Yuan, Z. Liu, G. Zhang, T. Zhang, Y. Qian, J. Wang, I. Lynch and Y. Deng, Highly fluorinated co-solvent enabling ether electrolyte for high-voltage lithium ion batteries with graphite anode, *Energy Mater.*, 2023, **3**, 300040.
45 K. Xu, Nonaqueous Liquid Electrolytes for Lithium-Based Rechargeable Batteries, *Chem. Rev.*, 2004, **104**, 4303–4418.
46 S. Tanuma, C. J. Powell and D. R. Penn, Calculations of electron inelastic mean free paths. V. Data for 14 organic compounds over the 50–2000 eV range, *Surf. Interface Anal.*, 1994, **21**, 165.
47 C. K. Powell and A. Jablonski, *NIST Electron Inelastic-Mean-Free-Path Database – Version 1.2*, National Institute of Standards and Technology, Gaithersburg, MD, 2010.